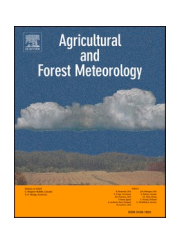
ELSEVIER

Contents lists available at ScienceDirect

Agricultural and Forest Meteorology

journal homepage: www.elsevier.com/locate/agrformet





Effects of spatial heterogeneity of leaf density and crown spacing of canopy patches on dry deposition rates

Theresia Yazbeck ^{a,*}, Gil Bohrer ^a, Chante' Vines ^a, Frederik De Roo ^{b,c}, Matthias Mauder ^b, Bhavik Bakshi ^d

- a Department of Civil, Environmental, and Geodetic Engineering, The Ohio State University, Columbus OH 43210, United States
- ^b Karlsruhe Institute of Technology, Institute of Meteorology and Climate Research Atmospheric Environmental Research, Garmisch-Partenkirchen, Germany
- ^c The Norwegian Meteorological Institute, 0313 Oslo, Norway
- d Lowrie Department of Chemical and Biomolecular Engineering, The Ohio State University, Columbus OH 43210, United States

ARTICLE INFO

Keywords: Canopy patches Leaf density Scalar flux Surface resistance

ABSTRACT

Trees have a large role in improving urban air quality, among other mechanisms, through dry deposition of scalars and aerosols on leaf surfaces. We tested the role of leaf density and canopy structure in modulating the rate of dry deposition. We simulated the interactions between a virtual forest patch and deposition rate of an arbitrary scalar using the Parallelized Large Eddy Simulation Model (PALM). Two canopy structures were considered: a homogenous canopy and canopy stripes. For each canopy stripe scenario, we considered thin, intermediate, and wide stripes, while the space between stripes equals the stripes' width. Four leaf area densities were considered for each case (LAI = 0.5, 1, 1.5, and 2). The results showed that denser canopies and canopy stripes experienced more total deposition, noting that stripes had a larger per leaf area deposition than homogeneous canopies. Our results can be explained by canopy-induced turbulence structures that couple the air within and above the canopy and lead to more effective leaf area where this coupling is stronger. We aggregate our results to the whole-patch scale and suggest a canopy-structure and leaf-area dependent correction to the canopy resistance parameter so to be used in coarse models that resolve dry deposition.

1. Introduction

Trees are essential in the regulation of air quality by uptake and emission of scalars, including air pollutants. It has been previously demonstrated that greenspaces management that includes trees in urban spaces is a potential strategy to improve air quality (Baró et al., 2014; Escobedo et al., 2008; Grote et al., 2016; Nowak et al., 2014). It has also been shown that forested greenbelts are particularly effective in regulating air quality around industrial sites (Gopalakrishnan et al., 2019). Techno-Ecological Synergy (TES) is an approach for designing sustainable industrial complexes. TES involves the ecosystem in improving the sustainability of an industrial design by taking advantage of existing synergies between technological and ecological systems, e.g. wastewater treatment through wetland ecosystem, freshwater availability from local watersheds, and air quality regulation by forest ecosystem (Gopalakrishnan et al., 2016; Gopalakrishnan and Bakshi, 2017).

Trees can improve air quality by dry deposition of pollutants on leaf

surfaces. Gaseous pollutants dry deposition occurs through leaves' stomata, while both and gas and particles adhere to leaves' surface through sorption and impaction (Nowak, 2002). Dry deposition in forest canopies has been studied extensively over the last decades (e.g., Hicks et al., 2016 and references within). Predicting dry deposition rates requires determining the aerodynamic resistance of the boundary layer, canopy air, skin-surface layer, and, for active uptake, stomatal resistance (Wesely and Hicks, 1977). These resistances are all modulated by leaf area density (Meyers et al., 1989) and atmospheric stability (Gronholm et al., 2009). Models for estimating dry deposition typically utilize the multiple resistance approach, where deposition rate is considered the inverse of the sum of the different resistances along the path of the deposited particle from the air to the leaf surface. They represent tree canopies either as a simplified big-leaf, or as a spatially uniform, vertically multi-layered model (Cherin et al., 2015; Hicks et al., 1987; Meyers and Baldocchi, 1988; Ruijgrok et al., 1997). Even the most advanced models, such as i-Tree Eco (Hirabayashi et al., 2012), which

E-mail addresses: yazbeck.3@osu.edu (T. Yazbeck), bohrer.17@osu.edu (G. Bohrer), vines.24@osu.edu (C. Vines), frederik.de.roo@met.no (F. De Roo), matthias. mauder@kit.edu (M. Mauder), bakshi.2@osu.edu (B. Bakshi).

 $^{^{\}star}$ Corresponding author.

provide highly resolved tree-level prediction of deposition rates by multiple pollutants, incorporate an implicit assumption of patch-level horizontal homogeneity of canopy structure, when scaling from the uptake by a single tree to uptake by a patch of trees. The finer details of the three-dimensional spatial structure and organization of the vegetation canopies is typically lost. Our study assesses the effect of spatial heterogeneity of leaf density and crown spacing of canopy patches on dry deposition rates in order to have a more efficient design of the forest ecosystem in regulating air quality around industrial complexes. We focus on the interactions between crown structure and aerodynamic resistance on passive dry deposition, and do not consider the added complexity of the dynamic chemistry, VOC emissions and active stomata uptake of atmospheric chemical.

Going beyond assumed spatial homogeneity requires a highresolution understanding of pollutants transport in the atmosphere and particularly through the canopy air space. Canopy-resolving large eddy simulations (LES) are developed to simulate deposition of scalars or particles in forests or agricultural vegetation canopies (Aylor, 2005; Bohrer et al., 2008; Boughton et al., 1987; Damschen et al., 2014; Raupach, 1989). LES can provide sufficient resolution to allow the investigation of the dynamics of scalar transport and uptake, while resolving the particular effects of canopy edges, turbulence in the canopy-roughness sublayer, and the empty spaces between canopies.

Canopy structure has a major contribution to the shape and intensity of turbulent motions through the formation of coherent eddies at the canopy scale (Raupach et al., 1996). These canopy-generated coherent eddies are integral to the transport of momentum and mass, including scalars, such as air pollutants (Finnigan et al., 2009; Gao et al., 1989). These interactions are further confounded by the structure, scale, and degree of spatial heterogeneity of the canopy roughness sublayer (Bohrer et al., 2009; Bou-Zeid et al., 2004; Sutherland et al., 2018). Several canopy characteristics were reported to affect scalar transport and surface uptake, including patch-scale canopy structure (patch shape and size, gap fraction, row spacing, etc.), tree-scale canopy structure (crown shape, stand density, species composition), and leaf-scale canopy properties, such as leaf skin characteristics, leaf shape and clumping, species-specific organic chemistry (Beckett et al., 2001; Cassiani et al., 2008; Dupont and Brunet, 2009, 2008; Dupont and Patton, 2012; Freer-Smith et al., 2004; Jones and Davies, 2017; Patton et al., 2011), which consequently affect dry deposition rate of scalars on trees.

Many earlier investigations attempted to study the effect of tree patches and densities on particle deposition, but were mostly focused on urban trees and street canyons (Gromke and Ruck, 2012; Morakinyo and Lam, 2016a, 2016b; Pugh et al., 2012; Salmond et al., 2013; Wania et al., 2012), while others focused on forest-edge effects on deposition, which was to experience the highest deposition in the forest (De Ridder et al., 2004; De Schrijver et al., 2007; Wuyts et al., 2008). Hicks (2008) showed that deposition on the forest edge was high and then decreased exponentially inside the canopy, where the number of crosswind edge per unit area of consideration was an important parameter in investigating edge effect on dry deposition. Tetzlaff et al. (2002) showed that inhomogeneity in forest edges induced more turbulent transport compared to homogeneous canopies. Therefore, surface resistance, i.e. deposition rate, was sensitive to forest patches and edges set up (De Jong and Klaassen, 1997). Similarly, leaf density influenced canopy induced turbulence, resulting in a non-linear effect between leaf area index (LAI) and deposition rate (Erisman and Draaijers, 2003), which was not well resolved by analytical model (Petroff et al., 2008). Katul et al. (2011) showed that near-constant leaf density profile resulted in low deposition, while concentrated foliage on top of the canopy increased deposition with increasing LAI.

The multiplicity of these characteristics, the complexity of the way they can interact, and the large range of scales over which these interactions are effective, make it hard to conduct real-world, controlled experiments that could isolate and quantify the role of each characteristic. Therefore, an *in-silico* LES-based approach is critical to studying the

effects of the canopy structure on scalar dry-deposition dynamics, and resolve the way in which specific canopy characteristics affect the ability of the canopies to uptake pollution.

In our study we are investigating the effect of canopy patches and density in a forest context on dry deposition, where tree greenbelts are located downstream of a gaseous (scalar) air pollution source. We used the PArallelized Large-eddy simulation Model (PALM) (Maronga et al., 2015), which simulates a passive scalar transported by wind and deposited on trees, and follows the Eulerian approach for transport of gas-phase scalars. We utilized PALM for virtual experiments studying the effects of canopy organization (homogeneous or rows, different row spacing) and density (high or low leaf area) on the dry deposition rates of an arbitrary scalar under stable and unstable atmospheric conditions. This experiment represents a scalar emitted from an arbitrary virtual industry stack, and transported toward a structured canopy array downwind. PALM output allow the analysis of scalar and momentum transport within the canopy roughness sublayer and sinks into the canopy. Therefore, the resulting scalar uptake by the different canopy setups and densities will allow us to identify the effects of different characteristics of vegetation canopy structure on aerodynamic resistance and the effectivity of the vegetation in pollutant removal.

2. Methodology

2.1. PALM

The PArallelized Large-eddy simulation Model (PALM) (Maronga et al., 2015) has been extensively used for simulation of turbulence in the atmospheric surface and boundary layers (e.g., Huq et al., 2018; Letzel et al., 2012; Park and Baik, 2014; Raasch et al., 2017; Raasch and Schröter, 2001). Several PALM-based studies explicitly investigated the interaction of forest canopy structure and the atmospheric boundary layer (Banerjee et al., 2017; Kröniger et al., 2018; Kurppa et al., 2018; Resler et al., 2017). PALM release 6.0 r4359 was used in this experiment. The PALM setup and user input files used for our simulations were included in the Supplementary Material.

PALM 6.0 has seven prognostic variables: the velocity components (u, v, and w), potential temperature, specific humidity, the subgrid-scale turbulent kinetic energy (TKE) and a passive scalar. All variables are on a Cartesian grid, but the velocities are staggered with respect to the scalar, with the staggering along their own direction. PALM utilizes the filtered, non-hydrostatic, incompressible Navier-Stokes equations in Boussinesq approximated form. While PALM can resolve moist atmosphere, we did not want uncertainty in vegetation transpiration and stomata conductance to affect our results and set up the simulation to run using dry air only. The governing equations for momentum, temperature and scalar in dry air simulations in the simulation domain are as following:

$$\frac{\partial \overline{u}_{i}}{\partial t} = -\frac{1}{\rho} \frac{\partial \overline{u}_{i} \overline{u}_{j}}{\partial x_{j}} - \varepsilon_{ijk} f_{j} \overline{u}_{k} + \varepsilon_{i3j} f_{3} u_{g,j} - \frac{\partial}{\partial x_{i}} \left(\frac{\pi^{*}}{\rho} \right) + g \frac{\overline{\theta}_{v} - \langle \theta_{v} \rangle}{\langle \theta_{v} \rangle} \delta_{i3}
- \frac{1}{\rho} \frac{\partial}{\partial x_{i}} \rho \left(\overline{u''_{i} u''_{j}} - \frac{2}{3} e \delta_{ij} \right) - c_{d} LAD \sqrt{\overline{u}_{k}} \overline{u}_{k}$$
(1)

$$\frac{\partial \overline{u}_j \rho}{\partial x} = 0 \tag{2}$$

$$\frac{\partial \overline{\theta}}{\partial t} = -\frac{1}{\rho} \frac{\partial \rho \overline{u}_j \overline{\theta}}{\partial x_j} - \frac{1}{\rho} \frac{\partial}{\partial x_j} \left(\rho \overline{u''_j \theta''} \right) + \frac{\partial Q_{\theta}}{\partial z}$$
(3)

$$\frac{\partial \overline{\varphi}}{\partial t} = -\frac{1}{\rho} \frac{\partial \rho \overline{u}_j \overline{\varphi}}{\partial x_j} - \frac{1}{\rho} \frac{\partial}{\partial x_j} \left(\rho \overline{u''_j \varphi''} \right) - c_{\varphi} LAD \sqrt{\overline{u}_k} \overline{u}_k \left(\overline{\varphi} - \varphi_{c,0} \right)$$
(4)

where $u_1 = u$, $u_2 = v$, and $u_3 = w$ are the velocity components [m s⁻¹], along the spatial axes coordinate $x_1 = x$, $x_2 = y$, and $x_3 = z$, [m], along the latitudinal (x, eastward), longitudinal (y, northward), and vertical

(z, upward) directions, respectively. An overbar marks the grid box resolved component, and a" marks sub-grid-scale perturbations from the resolved component.t is time [s], $f_i = \{0; 2\Omega\cos(\phi); 2\Omega\sin(\phi)\}$ is the Coriolis parameter [s⁻¹] with Ω =0.729 × 10⁻⁴ [rad s⁻¹] is the Earth's angular velocity and ϕ is the geographical latitude (55 degrees North in this case), $u_{e,i}$ are the geostrophic wind components [m s⁻¹], ρ is the basic density of dry air [kg m $^{-3}$], $\pi^* = p^* + \frac{2}{3}\rho_0 e$ is the modified perturbation pressure. p^* is the perturbation pressure [hPa], $e = \frac{1}{2}\overline{u''_i u''_j}$ is the subgrid-scale turbulent kinetic energy [m² s⁻²], which is prognosed by PALM's subgrid-scale turbulence scheme, θ is the potential temperature [K], θ_v is the virtual potential temperature [K], $\overline{u''_i\theta''}$ is the subgridscale diffusion of temperature, g is the gravitational acceleration [m s^2]. φ is the scalar concentration [kg m^3], $\overline{u''_j \varphi''}$ is subgrid-scale scalar diffusion, LAD is the leaf area density [m² m⁻³], c_d is the drag coefficient (dimensionless), c_{φ} is the scalar exchange coefficient (dimensionless), and $Q_{\theta}(z_c)$ is the heat flux on top of the canopy layer [K m s⁻¹] (Maronga et al., 2020, 2015). Water exchange between the canopy and atmosphere was not considered in our simulations, and latent heat flux was set to zero.

Discretization is applied throughout the PALM simulation domain by using the finite-differences approach on horizontally equidistant grid. PALM uses the Arakawa and Lamb (1977) type-C, staggered grid scheme. Numerical integration is done using an upwind-biased 5th order differencing scheme in combination with 3rd order Runge-Kutta time stepping. The time step is dynamic, and calculated based on maximal wind speeds in the previous time step, relative to grid spacing. Subgrid-scale diffusion terms for momentum and scalar are parametrized using a 1.5-order closure based on Deardorff (1980). PALM follows the modified method of Moeng and Wyngaard (1988) and Saiki et al. (2000). Under convective conditions, subgrid-scale diffusion is proportional to the geometric mean of the grid size (length scale) and to the root of the resolved turbulence kinetic energy (velocity scale).

PALM's canopy model calculates the exchange of momentum, scalar mass and heat between the canopy and the atmosphere over several vertical grid points layers, while taking into account the variation of drag induced leaf density within the canopy subdomain (below the top canopy height). The canopy is modeled as a porous medium, i.e. does not act like a wall but air can infiltrate into the canopy, and the leaf drag (last term of eq. 1) removes momentum from the flow (Shaw and Schumann, 1992; Watanabe, 2004). The canopy leaves are also considered a source or sink for heat (last terms of equations 3). For the vertical kinematic canopy heat flux, $\partial Q_{\theta}/\partial z$ [K m s⁻¹], PALM follows an exponential decay function proportional to the incoming shortwave solar radiation attenuation into the canopy, as in Brown and Covey (1966) (Maronga et al., 2015):

$$Q_{\theta}(z) = Q_{\theta}(z_c) exp(-\eta LAI(z))$$
(5)

where

$$LAI(z) = \int_{z}^{z_{c}} LAD \ dz \tag{6}$$

and z_c is the height of the top of the canopy, and η is a unitless coefficient for the rate of shortwave radiation extinction through the canopy, set to 0.6. The canopy effect on scalar is accounted for through the last term of Eq. 4, which follows the assumption that the scalar sink into the vegetation surface is proportional by the concentration gradient between the air and leaf surface (Maronga et al., 2015). Technically, the canopy could be a source for scalar if $\varphi < \varphi_{c,0}$ in Eq. 4. However, in our simulations, we set $\varphi_{c,0} = 0$, since we assume no scalar accumulation on scalar leaves, thus canopies are always acting as a sink for scalar.

2.2. Virtual experiment

Canopy patches considered were stripes of various densities and spacing, and homogeneous canopies of different densities under mild unstable boundary-layer conditions and stable conditions. We chose an arbitrary, but common, canopy structure expressed as a maximal leaf area of 4 and canopy top height of 20 m. While our simulations represent arbitrary virtual cases and do not represent any specific location, some needed details, such as the combination of wind speed, temperature and its vertical profile, incoming solar radiation and surface heat flux must be coordinated to form a realistic simulation case. These parameters were based on observations at an arbitrary day in a forest flux station in Indiana and a nearby airport sounding station in Ohio. Within the multitude of variables and dimensions that control surface-atmosphere interactions, we attempt to generalize our finding along two dimensions only - leaf density and row spacing (indicative of the lengthscale of surface heterogeneity, relative to canopy height). We added the PALM simulation-setup and user-domain-definition files for the simulations that were discussed in this manuscript in the Supplementary Material.

2.2.1. Domain

This virtual experiment aims at simulating the interaction of a downwind canopy with an arbitrary scalar, representing a virtual pollutant released from an upstream source. It is set up to study the effects of canopy density and spatial structure on the efficiency of these canopies at removing the scalar by dry deposition. A rectangular domain was considered, $96 \times 432 \times 192$ grid points with a $5 \times 5 \times 5$ m³ resolution, thus with dimensions of $480 \times 2160 \times 960$ m³ using the $x \times y \times z$ convention, where x is the eastward, y is the northward, and z the upward axes. The geostrophic wind aloft, directed along the y direction, and Coriolis formed Ekman-spiral rotation of the wind directions toward the domain floor. The canopy occupied the xy plane over the full width of the x dimension and from grid 288 to 432 (1440 m-2160m) at the y dimension (Fig. 1). The canopy was four grid layers (20 m) tall.

The simulation is initialized as vertically prescribed and horizontally homogenous profiles of wind speed and temperature. To reach realistic turbulence mixing and a stationary equilibrium vertical wind speed profile, we run for 6.5 hours of spin up time. Scalar release locations were prescribed at all elevations in a vertical rectangular prism located at grid coordinates [46:49, 5, 1:190] (grid numbers along the [x, y, z], directions, respectively). This scalar source is stationary, injecting scalar at a nominal rate of 0.001 [kg m⁻² s⁻¹] from each grid box, starting 5 hours into the simulation time (which is also an hour and a half before the end of spin up time). Therefore, during our 30 minutes' simulation (hours 6.5 to 7 of overall simulation time), we reach fully turbulent conditions and a realistically mixed scalar background concentration. It is noteworthy that a wider scalar-source column (along the x dimension) would have helped reaching a well-mixed background concentration faster, however, in PALM, scalar sources are assumed to represent physical structures and, therefore, it acts as a barrier for the wind (i.e. a physical "wall") which significantly affects the wind distribution at the downwind direction. To minimize such effect, we used a very narrow (4 grid wide) "Scalar Column". The canopy was located around 1.3 km north of the scalar source to allow it to mix vertically and horizontally. Our analysis shows that the scalar concentration is well mixed when it hits the canopy as shown in Fig. 2. Lateral boundary conditions are cyclic for all variables, including scalar. Top boundary conditions for momentum and scalar are free-slip and Neumann for potential temperature with a prescribed gradient based on the initial profile. Bottom boundary conditions for momentum are no-slip with a Monin-Obukhov based flux prescribed at the surface grid. Bottom boundary conditions for all other variables are free slip, with surface fluxes prescribed as sink terms over the entire horizontal and vertical extent of the canopy subdomain. Other variables boundary conditions are listed in the Supplementary Material. Surface flux of scalar is prescribed as a sink term

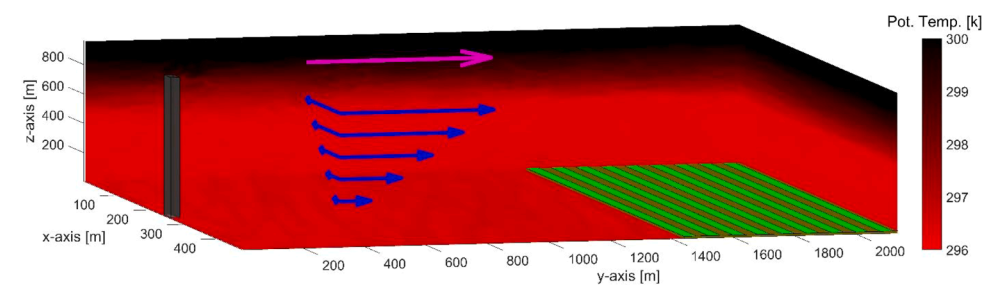


Fig. 1. Outline of the 3D simulation domain. Canopy-containing grid boxes for the homogenous cases are illustrated in green (both dark and green), and orientation of the edges of canopy stripes in the Str2h case are illustrated in light green. Geostrophic wind forcing direction and speed is indicated by the magenta top arrow (forcing aloft). Blue arrows represent the horizontal averaged u and v wind components at different elevations, which resulted from the wind forcing aloft and Coriolis force. Scalar is released from a vertical column (grey) 25 meters (5 grid points) from the upwind boundary

of the model and at all elevations from z=0.960 [m above ground]. The red background represents an instantaneous snapshot of potential temperature at the west, north and surface boundaries at the start of data analysis period (last 30 min of simulation) (red-scale color bar [k]).

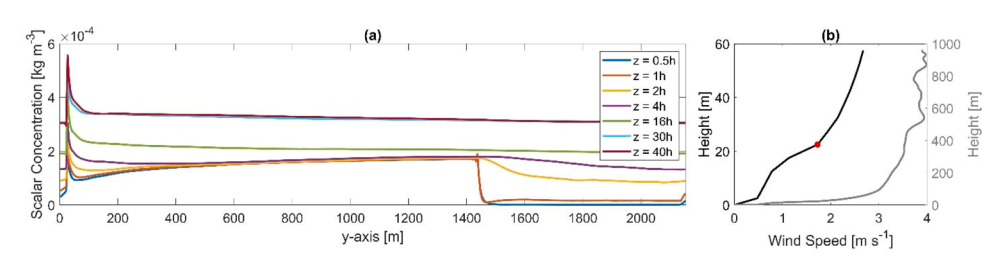


Fig. 2. (a) Scalar Concentration along the y-axis at different heights. Heights are normalized by canopy height, h. Scalar concentration is averaged along the x-axis and during the analysis portion of the simulation time (last 30min). (b) Wind speed profiles along the bottom 60m of the simulation domain (left vertical axis of the panel) and along the full height of the simulation domain (right vertical axis of the panel). The red dot marks the aerodynamic height of the canopy, as detected by the in-

flection point of the wind-speed profile. Both plots are for the case of homogeneous canopy with LAI = 1.5.

throughout the canopy sub-domain. Thus, all released scalar that was not absorbed by the surface stays in the model. While that leads to a slow buildup of scalar concentration throughout the simulation domain, the purpose of this study is to compare among the effects of different canopy structures and densities on dry deposition, thus, we are comparing scalar uptake rates among cases of different canopy structure but identical scalar release rate. Our results confirm that scalar concentration shortly upwind of the first canopy edge is consistent among the different simulations, though not equal. Upwind scalar concentration slightly differs among different canopy patches and densities, but with minimal effect on deposition rates.

2.2.2. Initial conditions

We simulate an arbitrary, characteristic, clear-sky, summer day under mildly unstable conditions. We also include a limited set of two simulation cases under stable conditions. We used observations to define such realistic combination of meteorological conditions. These conditions are manifested in the input through prescribing the initial horizontal wind, humidity and potential temperature profiles, which define the height of the boundary layer, and the surface fluxes of sensible and latent heat, which combine with the wind profile to define the stability condition. The wind profile used at initialization was further used as the geostrophic wind profile for lateral wind forcing during the simulation.

2.2.2.1. Potential temperature profile. Upper-atmosphere potential temperature profile data was processed based on the National Oceanic and Atmospheric Administration (NOAA) radiosonde database, "NOAA/ESRL Radiosonde Database," 2019) from Wilmington OH (Station ID WBAN:13841). Observations are provided on a daily basis, at 7:00 am and 7:00 pm local time, and the average profile for summertime morning data was considered for unstable simulations and after noon data were used for stable. Summer potential temperature profiles up to 3000m height were studied from year 2014 till 2017.

The profile was divided into three layers: surface layer, mixing layer, and free atmosphere. We idealized the initial atmospheric temperature profile using a different slope for each layer, while keeping the slope constant within each of the layers. In the free atmosphere, we set the slope of potential temperature increase with height equal to adiabatic

slope, $0.01~[\mathrm{Km}^{-1}]$. In the mixing layer, we set the potential temperature constant (slope = 0). At the surface layer we set the slope of potential temperature based on the average observed near-surface slope from sounding. The full potential temperature profile input is presented in Table 1.

2.2.2.2. Forcing. The forcing considered are to simulate atmospheric conditions in Cincinnati Ohio, and while the location is arbitrary and have no particular importance to our analysis, our project was inspired by an actual case at that location. Thus, input data were taken from stations close to that geographic area. The sensible heat fluxes and surface temperature data were taken from the AmeriFlux database for the Morgan Monroe State Forest site in Indiana, site ID: US-MMS (Novick and Phillips, 2020). An arbitrary summer day without precipitation was picked, 08/01/2014, and near-surface air temperature, radiation and heat fluxes were based on the observations for the morning time of that day. Geostrophic wind was forced as $u_{8,2} = 4 \, [\text{m s}^{-1}]$ and $u_{8,1} = 0 \, [\text{m s}^{-1}]$, where, $u_{8,2}$, was oriented northward. As for the scalar flux, an arbitrary flux rate = 0.001 [kg m⁻² s⁻¹] was prescribed. All initial parameters and forcing are summarized in Table 1. All simulations assumed the same, flat topography. The effect of Coriolis force was

Table 1 Forcing for all simulation cases.

Parameter	Unstable	Stable
Sensible heat flux (integrated from ground surface to canopy top) [W m ⁻²]	14.329	-24.085
Initial potential temperature at surface [K]	295.45	292.81
Initial potential temperature profile	-0.0001; 0.00;	0.07;0.00;0.01
gradients [K m ⁻¹]	0.01	
Potential temperature profile gradients	0:75; 80:395;	0:75; 80:395;
levels [m]	400:960	400:960
Geostrophic wind V-component [m s ⁻¹]	4.0	4.0
Geostrophic wind U-component [m s ⁻¹]	0.0	0.0
Scalar flux (at each grid box that releases scalar) [kg m $^{-2}$ s $^{-1}$]	0.001	0.001
Leaf drag coefficient, c _d [dimensionless]	0.15	0.15
Scalar exchange coefficient, c_{φ} [dimensionless]	1	1

included in the simulation dynamics, using the default PALM setup. Fig. 2 (a) shows the scalar concentration along the model y-axis, where it could be seen that inside the canopy scalar concentration significantly drops while as going up in height the drop in scalar concentration is less significant.

2.2.3. Canopy setup

Four virtual canopy structures were considered: (i) homogeneous canopy (Hom); and canopy stripes oriented along the x-axis (Table 1). The interaction between Coriolis and surface drag produced a rotation of the flow field (Ekman spiral) that resulted in an incident angle close to a diagonal at the height of the canopy top for all patches, thus, strip orientation formed an angle with the incident wind direction at that height. Three different stripe widths were considered: (ii) 0.5h (Str0.5h); (iii) 1h (Str1h); and (iv) 2h (Str2h), where h=20 [m] is the canopy height. The width of spaces between stripes was equal to the stripe width.

Four leaf-density levels were considered for each canopy structure: LAI = 0.5; 1; 1.5; and 2 $[m^2_{leaf} m^2_{ground}]$. It is important to note that LAI represent the average leaf area per ground area, and therefore, it is a scale-dependent property, which depends of the ground area that the leaf area is averaged over. For example, in the densest striped case, LAI within forested columns was 4, and between the stripes it was 0, averaging over the whole model domain that represents the canopy (including both tree and empty stripes) LAI average to 2. This creates a fundamental difference regarding leaf area density between the homogenous canopy where leaves are evenly spread and the striped canopies where leaves only occupy half of the canopy area. While the whole-canopy domain-average leaf area in the homogeneous and striped cases are the same, the leaf density within the forested locations in the striped cases is double that of the corresponding homogeneous canopy. To enable a comparison between striped and homogenous cases in terms of both mean leaf area and within-crown leaf density, we added two additional cases of homogeneous canopy with LAI of 3 and 4. These represent cases where leaf density in the forested parts matches that of the striped cases with whole-canopy average LAI of 1.5 and 2, respectively. Naturally, there could be an infinite number of canopy organizations. Canopy can cluster at other shapes than stripes, in blocks and circles, and irregular patches. In this study, we focus on canopy stripes. We chose this focus because canopy stripes are relatively common, for example, in orchards and boulevards. The LAI and canopy height were constant within a row (or throughout, in the homogeneous cases), while vertically, a leaf area density (LAD) profile was prescribed for each canopy level. LAD profile is vertically integrated to LAI. The different LAD profiles had similar normalized shape (per unit LAI and height) based on a default LAD profile provided by PALM. The discrete LAD profiles within our simulation vertical grid spacing were slightly changed among different LAI cases so that the profiles willvertically integrate to the prescribed LAI for the case. These LAD profiles are shown in Fig. 3. The leaf-drag coefficient was set as $c_d = 0.15$, which is the default value used in PALM. PALM uses a dimensionless leaf-scalar exchange coefficient. As this is a purely virtual case, we chose the simple assumption of no scalar accumulation on the leaf surfaces (effectively, zero scalar concentration at the leaf surface) and an arbitrary scalar exchange coefficient value $c_{\varphi} = 1$.

3. Results

Instantaneous snapshots of prognostic variable values were output every 5 seconds throughout the last 1800 seconds of simulation time. Instantaneous deposition rate was calculated using these output data. Scalar fluxes were calculated as the covariance between vertical wind component and scalar concentration. We used the difference between the value at each grid point throughout the simulation domain and the spatial and temporal means over the 30 minutes' simulation time at each horizontal grid layer to get the instantaneous deviation from the mean

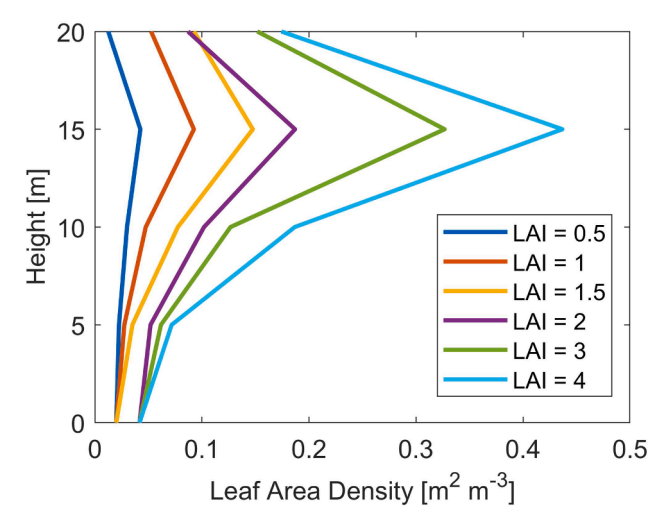


Fig. 3. Leaf area density profiles for the simulation cases with different LAI.

vertical wind velocity and scalar concentration. At each grid, the temporal average of the products of these vertical wind and scalar concentration deviations provides their covariance at that grid point. We averaged the grid-level covariances over space (within each horizontal grid layer) to get the vertical profile of the scalar flux during the 30 minutes' simulation.

For each of the instantaneous outputs at each grid point, the deposition rate, $\frac{F_{\phi}}{\Delta z} [kg \, m^{-3} \, s^{-1}]$ was calculated using the sink term in Eq. (4), i. e.:

$$\frac{F_{\varphi}}{\Delta z} = -c_{\varphi} LAD \sqrt{\left(\overline{u}_{k}\overline{u}_{k}\right)} \left(\overline{\varphi} - \varphi_{c,0}\right) \tag{7}$$

where F_{φ} [kg m⁻² s⁻¹] is the flux of scalar at each canopy grid, $\Delta z=5$ [m] is the vertical grid spacing. The last term of Eq. 4 is a volumetric scalar concentration term per time, thus multiplying it by height will result in a scalar flux term noted as F_{φ} . In this study, we ignore scalar chemistry and therefore assume that surface reactions do not enhance or limit the deposition rate, i.e., $\varphi_{c,0}=0$. c_{φ} [unitless] is the leaf-surface aerodynamic conductivity to transport of the scalar. Then, the total surface flux of scalar due to deposition on canopy surfaces, $F_{s\varphi}$ [kg m⁻² s⁻¹] was calculated as

$$F_{s\varphi} = h \left\langle \sum_{z=0}^{h} \frac{F_{\varphi}}{\Delta z} \right\rangle \tag{8}$$

where $\langle \rangle$ marks spatiotemporal average over the horizontal domain (though $F_{\varphi} \neq 0$ only in the "forested" parts of the domain, i.e., columns that contain canopy) and over the 30 minutes simulation analysis period, and h is the canopy height. Fig. 4 shows the results for the total deposition for the 18 simulations.

The average deposition in a striped canopy structure was larger than in homogeneous canopies with similar plot-level leaf area. Total deposition increased with increasing LAI, but that increase did not scale linearly with leaf area. Increasing leaf area increased deposition in both homogeneous and stripped canopies, while this increase was more intense in the stripes case. A four-fold increase of leaf area, from 0.5 to 2, resulted only in a 24% increase in deposition rate for homogeneous canopy, and in 108% in intermediate stripes (Str1h). As for spatial heterogeneity of deposition rates within the canopy, the highest deposition is occurring at the forward-facing edges of canopy stripes (Fig. 5). In the canopy stripes, wind speed and scalar concentration are decreasing as the wind penetrates deeper across the width of each canopy stripe while encountering drag and depositing scalar on leaves. Wind speed and scalar concentration then increase in the empty gap

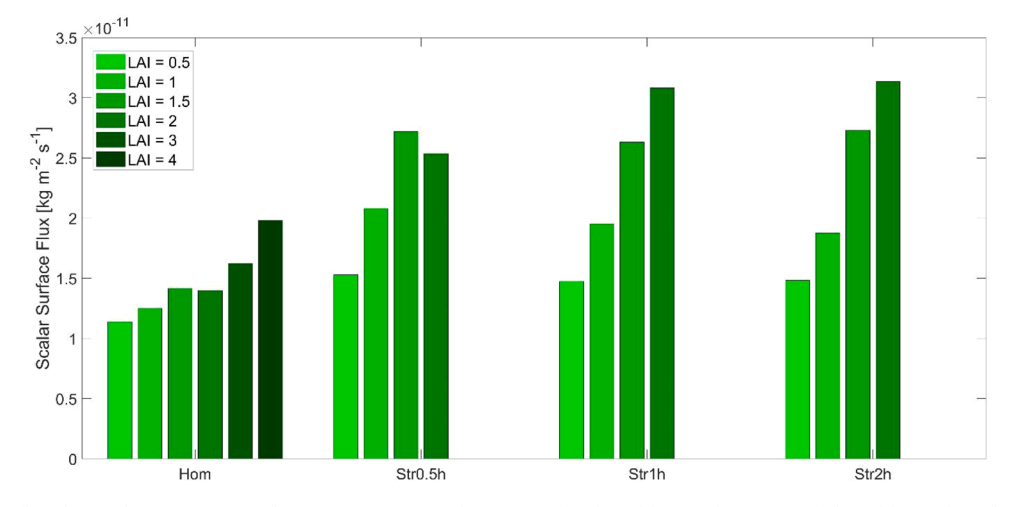


Fig. 4. Scalar surface flux due to deposition: Hom (homogeneous), Str0.5h (stripes of 0.5h width), Str1h (stripes of 1h width), and Str2h (stripes of 2h width).

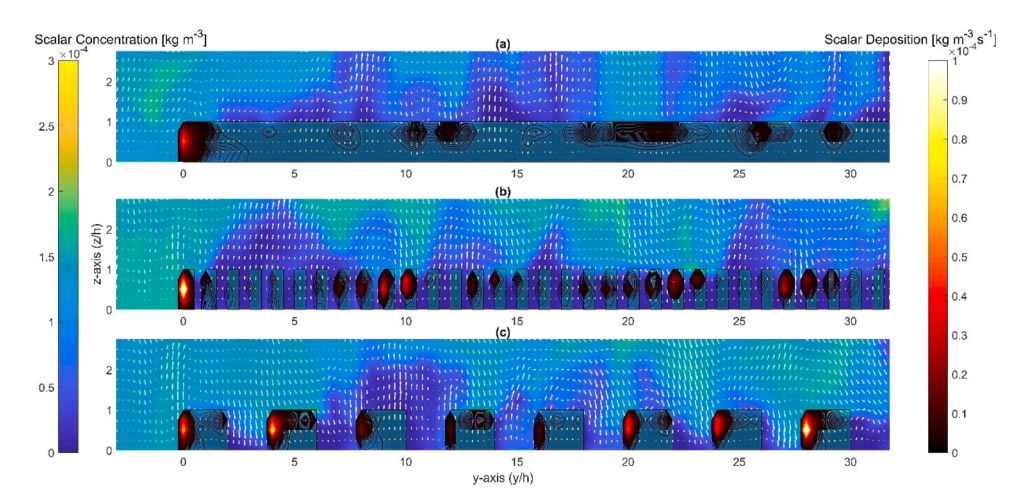


Fig. 5. Y-Z instantaneous cross section showing only the canopy portion of the simulation domain. The figure's horizontal axis refers to the model's y-axis normalized by canopy height (i. e. y/h) and starting from the upwind canopy edge. The Figure's vertical axis is the model's zaxis normalized by canopy height, (i.e. z/h) starting from the ground. The background (left color bar) is the scalar concentration [kg m⁻³] while the contour lines (right color bar) represent the deposition rate of scalar on the canopy [kg m⁻³ s⁻¹]. The shaded areas represent the forested parts of the simulation domain. The white arrows are the v-w wind vectors, where, for the purpose of illustration, the vertical (w) component is scaled 5x relative to the horizontal (v). (a) Homogeneous canopy, (b) Narrow canopy stripes Str0.5h, and (c) Wide canopy stripes, Str2h. All three canopies have plot-level average LAI = 1.5.

before hitting the next canopy stripe (Fig. 6). That covariance of wind and scalar concentration makes the first row of upwind leaves of each canopy stripe encounter a higher scalar concentration coupled with a higher wind speed, leading to a high deposition rate. The spatial structure of the striped canopy allows this process to repeat making the

stripes more efficient at dry deposition than homogeneous canopies. This "recharging cycle", however, is more efficient in the dense wider stripes, leading to overall highest deposition rates at the dense Str1h and Str2h cases (Fig. 4).

Homogeneous canopies under stable conditions showed lower

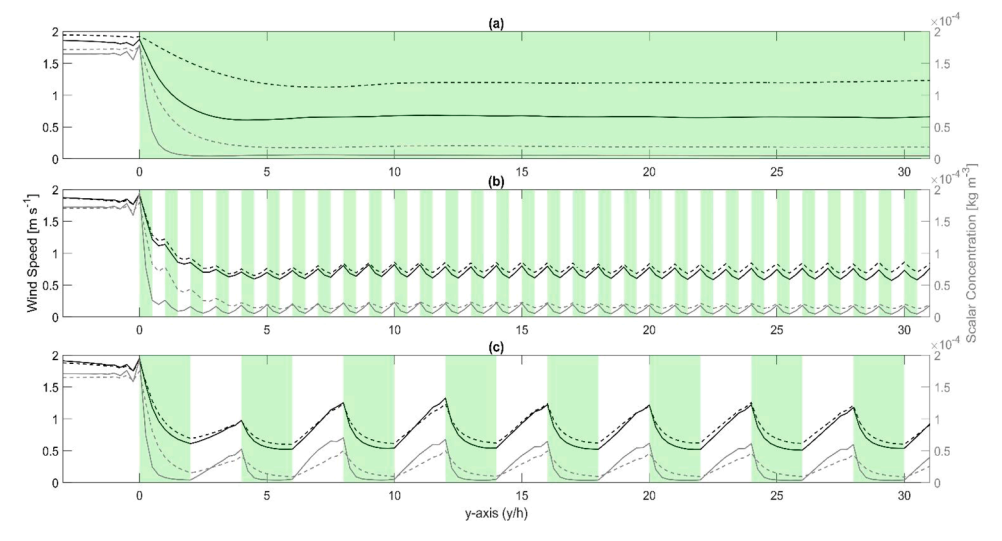


Fig. 6. Time-averaged wind speed (black lines, left vertical axes) and scalar variations (grey lines, right vertical axes) over the 1800 seconds simulation time inside the canopy. Average was performed over the whole east-west direction and entire canopy height in z-direction. The figure's horizontal axis refers to the model's vaxis normalized by canopy height (h) and starting from the canopy edge, i.e. 0 tick defines the first canopy edge that faces downwind. Green fill presents the canopy footprint along the y-axis. (a) Homogeneous canopy, (b) Narrow canopy stripes, and (c) Wide canopy stripes. Dashed lines represents canopy of LAI = 0.5, and solid line represents LAI = 2. The downwind axis is normalized by canopy height, where 0 indicates the first canopy edge facing the wind flow.

deposition rate (30% less deposition) than the same canopy setup under mild unstable conditions, due to decoupling of the canopy air space that developed under stable conditions (Fig. 7 (a)). In canopy stripes, shear induced turbulence due to the presence of stripes was prevailing source of turbulence in both stable and unstable conditions, which generated significant vertical mixing allowing both atmospheric conditions to have close deposition rates (Fig. 7 (b)). Thus, since both stable and unstable conditions resulted in close deposition except for homogeneous canopies, through the discussion, we will focus the analysis on unstable conditions.

4. Discussion

We found that both leaf area and row spacing affected the scalar deposition rates. It is indeed expected that leaf area will increase deposition, as it is explicitly and linearly represented in the deposition equation Eqs. 4,(7) (Hirabayashi et al., 2011; Liu et al., 2018; Wedding et al., 1977). However, high-frequency covariance between the spatial variations of wind speed and scalar concentration may lead to accumulation of the linear effects that control scalar deposition at the grid-scale into non-linear effects at the whole-canopy scale. The reason for such non-linear effects is that not all leaves meet the same scalar concentrations or wind speeds (Wiman and Ågren, 1985). Adding leaves at the top of the canopy, where wind is fast and scalar concentration is high will be more effective than adding leaves near the ground. Similarly leaves at the upwind-facing edge of a canopy stripe will encounter higher scalar concentration at higher wind speeds than the same leaf area further downwind (Fig. 6). This coupling of high scalar concentration with high wind speed leads to a further higher deposition since this latter is proportional to both scalar and wind (Eq. 7).

The interaction between the canopy surface and the atmosphere is dominated by coherent eddy structures. These structures are manifested through pairs of head-up and head-down vortices that induce ejections (strong bursts) and sweep (gusts) from and into the canopy, respectively (Finnigan et al., 2009; Katul et al., 1997; Raupach and Thom, 1981). Momentum transfer can be dominated by either sweeps or ejections. In order to determine how the momentum transport is occurring, we conducted quadrant analysis, to compute ΔS_0 , an index of the sweep dominance (following, Katul et al. 2006):

$$\Delta S_0 = \frac{\langle \overline{v_r'} \overline{w'} \rangle_{IV} - \langle \overline{v_r'} \overline{w'} \rangle_{II}}{\langle \overline{v_r'} \overline{w'} \rangle}$$

$$\tag{9}$$

where a single prime marks the grid-box level resolved perturbation from the horizontal spatiotemporal mean of a property. $\overline{v_r}$ is the wind velocity component at the rotated downstream direction, defined by the domain-wise mean wind direction at the canopy-top elevation. $\langle \overline{v_r}^{'} \overline{w}^{'} \rangle_{\text{IV}} / \langle \overline{v_r}^{'} \overline{w}^{'} \rangle_{\text{II}} / \langle \overline{v_r}^{'} \overline{w}^{'} \rangle$ are the stress fractions in the fourth $(\overline{v_r}^{'} \text{ is positive and } \overline{w}^{'} \text{ is negative, representing sweeps)}$ and second quadrant

 $(\overline{v_r}')$ is negative and \overline{w}' is positive, representing ejections), respectively. Therefore, sweeps dominate momentum transfer when $\Delta S_0 > 0$ and ejections dominate when $\Delta S_0 < 0$ (Katul et al., 1997, 2006). Fig. 8 shows ΔS_0 at the top of the canopy for different canopy structures. In the canopy stripes (Fig. 8 (c-d)), we can see that ejections happen to be mostly in canopy stripes, right after the canopy edge while sweeps happen in empty stripes. Therefore, "dirty" air from above is being swept into the empty spaces between stripes, then "cleaned up" by deposition as it passes through canopy stripes, resulting in a more efficient dry deposition in canopy stripes patches. The spatial coordination between the ejection/sweep locations and the canopy stripes (as was also observed by Bohrer et al., (2009)) further enhances the non-linear effects of the interactions between canopy location and scalar concentration.

We found strong ejections at the first upwind canopy edge of all canopy structures (Figs. 5, 8). We found an enhanced uplift zone extending from the upwind edge of the canopy to about 1.5-3h downwind from the edge for sparse-dense canopies, respectively. An uplift zone near the upwind edge of a backward facing step is expected, and was reported for sparse, canopy-like steps by Chatziefstratiou et al. (2014). This uplift zone is then followed by an enhanced gust zone, further downwind the canopy (Dupont and Brunet, 2009). ΔS_0 tends to be negative near the upwind edge of the canopy, while further downstream (between 1h and 2h downwind of the canopy edge, into the y-axis direction) ΔS_0 becomes mostly positive, marking the development of an enhanced gust zone in our simulation results, where strong gusts are present, followed by a region dominated by ejections where to ΔS_0 is again negative.

Further downwind (>5h) from the canopy edge, the canopy structure affects the spatial organization of the ejection/sweep locations. We found that canopy stripes tend to organize the ejections, and, especially wide stripes, lead to co-location of more frequent and stronger ejections directly above the forested part of the canopy stripe than above the gap between the stripes (Fig. 8 (d)). This effect is not as strong in narrower stripes and the ejection-sweep distribution in the Str0.5h case (canopy structure with the narrowest stripes) is less coordinated with canopy stripe structure than in wider stripes (Str1h is not shown in Fig. 8).

Ejection and sweep intensities vary with LAI. Fig. 9 (a) shows that fraction of sweeps over the canopy decreases with increasing LAI across all canopy patches, thus LAI encourages more ejections across the canopy. Ejections are characterized to be strong burst thus enhancing turbulent mixing between canopy and air above.

We used a relatively high-resolution (5 m) LES simulations to explicitly resolve the momentum-canopy-concentration interactions that drive the dry deposition rates. However, such high resolution approach is not feasible for most applications, because the high computational demands limit its application over large domains and long periods. It is possible that our model resolution may not be suffi-

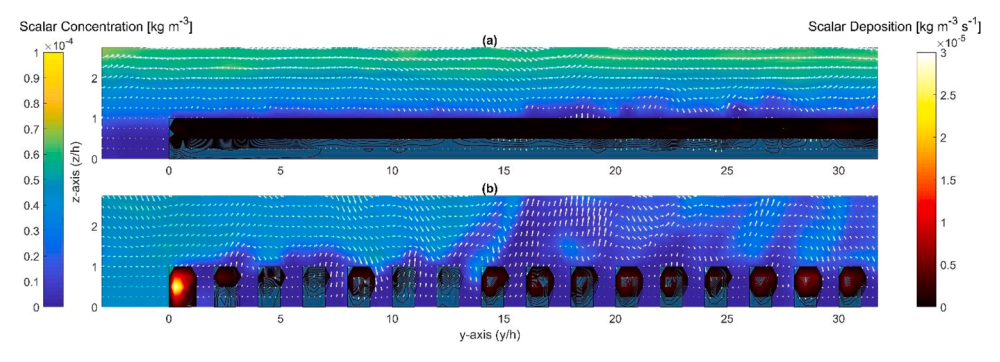


Fig. 7. Y-Z instantaneous cross section along the y-axis showing only the canopy portion of the simulation domain. The figure's horizontal axis refers to the model's y-axis normalized by canopy height (i.e. y/h) and starting from the upwind canopy edge. The Figure's vertical axis is the model's z-axis normalized by canopy height, (i.e. z/h) starting from the ground. The background (left color bar) is the scalar concentration [kg m⁻³] while the contour lines (right color bar) represent the deposition rate of scalar on the canopy [kg m⁻³ s⁻¹]. The shaded areas represent the forested parts of the simulation domain. The white arrows are the v-w wind vector, where, for the purpose of illustration, the vertical (w) component is scaled 5x

relative to the horizontal (v). (a) Homogeneous canopy under stable conditions, and (b) Intermediate canopy stripes Str1h under stable conditions.

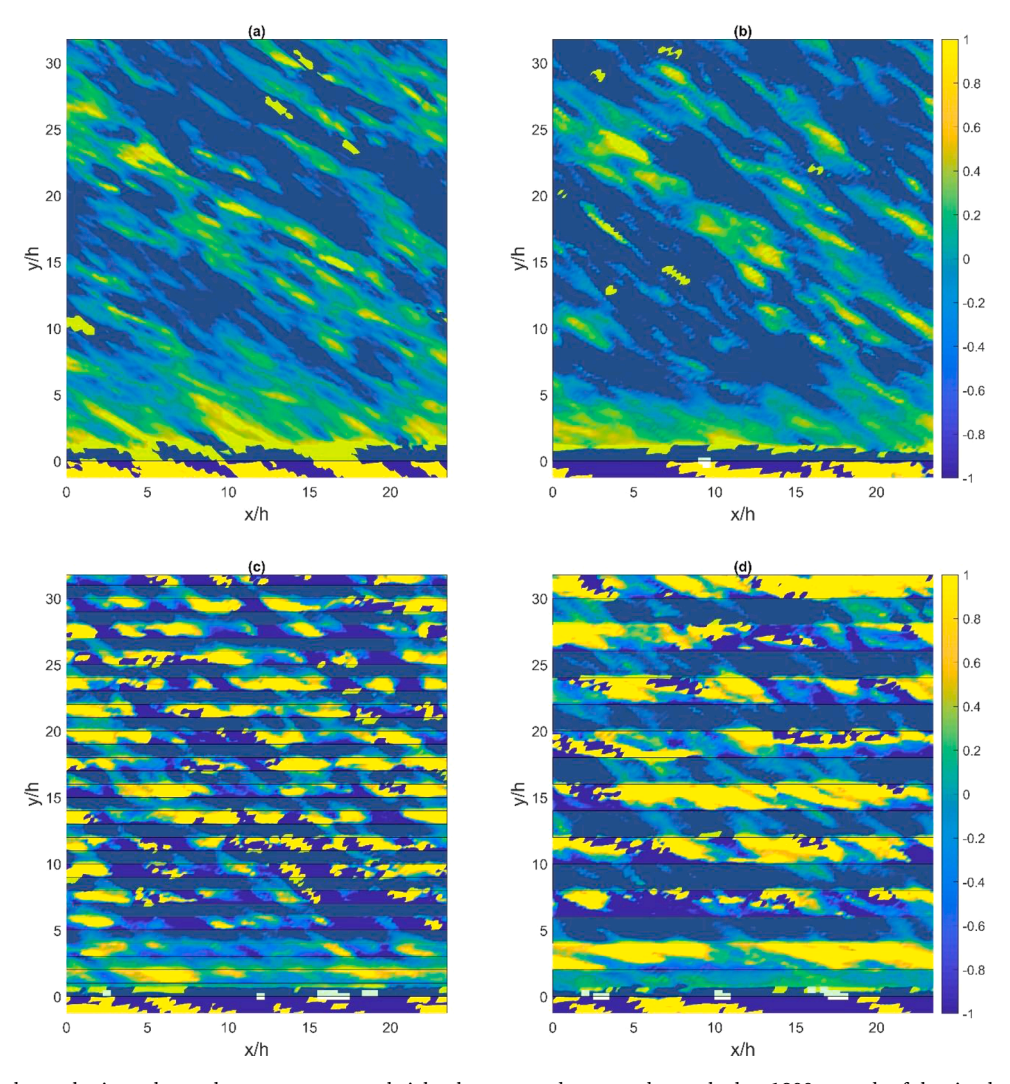


Fig. 8. ΔS_0 computed along a horizontal, x-y plane, at one canopy height above ground, averaged over the last 1800 seconds of the simulation. (a) Homogeneous canopy LAI = 1, (b), Homogeneous canopy LAI = 2, (c) Intermediate canopy stripes, Str1h, LAI = 2 (d) Wide Canopy stripes, Str2h, LAI = 2. The light green fill represents the canopy footprint.

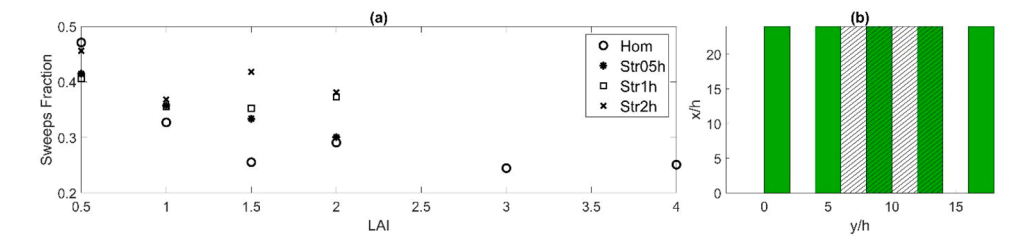


Fig. 9. (a) Fraction of sweeps out of both ejection and sweeps structures at 10h into the canopy. Spatial average of $\overline{\Delta S_0}$ was calculated over the whole y-axis (480m), a height going from 0 to 1.5h (0-30m), and along a band of 8h (160m) width in the northward centered at 10h (200m) into the canopy. The band has the same number of canopy stripes and empty stripes in the non-homogeneous cases. (b) XY section of Str2h case illustrating the band (hatched section) over which $\overline{\Delta S_0}$ was calculated. Both axes

are normalized by canopy height h.

cient to resolve the full details of the shear layer at the top of the canopy (Ross, 2008). Nonetheless, our model resolution is high enough to resolve the main component of the eddy motion within and above the canopy, as indicated by the inflection point at aerodynamic canopy height (Fig. 2 (b)). Typically, in regional and global atmospheric models, and in large-scale deposition models, such as i-TREE (Hirabayashi et al., 2015), the grid resolution is coarse to the degree that surface fluxes must be parameterized, and cannot explicitly resolve the effect of small-scale interactions between canopy structure heterogeneity, and turbulence transport and momentum. One common parameterization approach (e. g., the one used in the models: i-TREE (Hirabayashi et al., 2015), UFORE

(Nowak and Crane, 2000), and LUR (Bottalico et al., 2016)) is to represent the surface scalar flux, F_c , as:

$$F_c = v_d \Delta C \tag{10}$$

where

$$v_d = \frac{1}{r + r} \tag{11}$$

where v_d [m s⁻¹] is the conductance (also, deposition velocity), ΔC [kg m⁻³] is the concentration gradient between the boundary layer and leaf

surface. Usually, in models such as i-tree, v_d is the inverse of the sum of the resistances: aerodynamic, boundary layer, and canopy resistances (Hirabayashi et al., 2015). In our formulation of v_d , we considered the boundary layer aerodynamic resistance r_a and canopy resistance r_c .

We propose an approach to translate LES results into a whole-domain form equivalent to the representation of our entire domain in a coarse model. First, we calculated the mean high-resolution surface scalar flux on top of the canopy, i.e. the scalar flux into the canopy, within the canopy footprint, $F_{s\varphi}$ [kg m $^{-2}$ s $^{-1}$], from our model outputs using Eq. 8. On the other hand, $F_{s\varphi}$ could be calculated as:

$$F_{s\varphi} \approx v_d \left(\langle \overline{\varphi} \rangle \right|_{150m}^{300m} - \varphi_{c,0}$$
 (12)

where it is equivalent to a scalar gradient between the mixed layer above the canopy, $\langle \overline{\varphi} \rangle |_{150\text{m}}^{300\text{m}}$, and the canopy surface, $\varphi_{c,0}$, which is 0 in our case. The operator $\langle \rangle |_{150\text{m}}^{300\text{m}}$ marks spatial and temporal averaging over the domain width and height levels between 300 and 150 m above ground, which in our simulations mark the mixed layer near the upper parts of the planetary boundary layer, above the surface roughness sub-layer, where u^* is nearly constant. Thus, a coarse-scale equivalent of the scalar deposition rates in our simulation results, analogous to Eq. (10) is:

We can approximate a bulk r_a for our simulation domain using a u/u*2 dependent formulation (Monteith and Unsworth, 1990):

$$r_a = r_{aM} + r_b = \left(\frac{\langle \overline{u} \rangle|_{150m}^{300m}}{u^{*2}} + \frac{6.2}{u^{*(2/3)}}\right)$$
 (13)

where r_{aM} is the aerodynamic resistance to surface transport of momentum, and r_b is the access resistance to transport of a scalar. We can express canopy resistance to scalar transport, r_c , as the sum of two serial resistances proportional to leaf area:

$$r_c = \frac{r_{cA} + r_{cS}}{u^* LAI} \tag{14}$$

where r_{cA} [dimensionless] is the resistance coefficient for moving a scalar from the open atmosphere at the aerodynamic surface height (just above the canopy) into the canopy air, and r_{cS} [dimensionless] is the resistance of the leaf skin surface to scalar deposition.

We can then cast v_d is terms that are computed by our simulations:

$$v_d = \frac{1}{r_a + r_c} = \frac{u^* LAI}{u^* LAI \left(\frac{\langle \overline{u} \rangle_{150m}^{300m}}{u^{*2}} + \frac{6.2}{u^{*(2/3)}}\right) + r_{cA} + 1}.$$
 (15)

Consistent with coarse models, such as PALM's formulation of Eq. (6) and our setup of canopy resistance $r_{cS} = c_{\varphi} = 1$. Provided the simulation results, equations 11–16 can be solved to determine r_{cA} . This resistance term accounts for the LES-resolved effects per leaf area of small-scale, high-frequency, turbulence-canopy-concentration interactions on the effective overall conductance of scalar from the boundary layer to the leaf surface:

$$r_{cA} = u^* LAI \left[\frac{\langle \overline{\varphi} \rangle|_{150m}^{300m}}{F_{s\varphi}} - \left(\frac{\langle \overline{u} \rangle|_{150m}^{300m}}{u^{*2}} + \frac{6.2}{u^{*(2/3)}} \right) - \frac{1}{u^* LAI} \right].$$
 (16)

Wesely and Hicks (1977) derived a commonly used approach to parameterize surface resistance to mass exchange between canopy layer and atmosphere using the surface transfer function, B^{-1} , defined as

$$kB^{-1} = ku^*r_s \tag{17}$$

where k is the von Karman constant and r_s is the surface resistance which is associated with material transfer from air to surface component that is in contact with and is in [m s⁻¹], and which we defined as r_{cs} in our derivation of resistances. Thus, using analogy between r_s and r_c , we can further relate r_c to the common parameter for the surface transfer coefficient, B⁻¹, as:

$$B^{-1} = u^* r_c = \frac{r_{cS} + r_{cA}}{LAI} + \frac{r_{cA}}{LAI}.$$
 (18)

And while there are many alternative formulations for B⁻¹ (based on roughness length, friction velocity, and Schmidt number, e.g., (Chamberlain, 1966; Garratt and Hicks, 1973), the first term of the right hand side of Eq. (18), namely the leaf skin resistance, is already addressed by these formulations. Therefore, including the last term on the right hand side, the canopy air resistance, which was calculated in Eq. (16), could provide a correction term to the currently utilized B⁻¹. This correction term would represent an approach to utilize LES results for parameterizing the large-scale effects of canopy patch structure and, thus, improve large-scale models estimation of dry deposition over areas with heterogeneous vegetation.

Our study show that, for a given canopy structure, r_{cA} could be approximated as a linear function of LAI (Fig. 10). In homogeneous canopies, at least within the range of LAI between 0.5 and 4 (which is the common range for vegetation, except the tropics where LAI can be as high as 10) any addition of LAI is increasing the resistance per leaf area and making the canopy relatively less effective in removing scalar. However, in striped canopies, adding LAI decreases the resistance per leaf area, and the dense stripes are more effective in scalar removal than the sparse ones of the same structure (Fig. 4). Thus, total deposition for homogeneous canopies increases with LAI at a lower rate than for canopies stripes (Fig. 4). The non-zero slopes in Fig. 10 (a) prove the nonlinearity between leaf area density and dry deposition rate. The effect of patches is further emphasized in Fig. 10 (b), where similar trends are observed for a given LAI when going from homogeneous to structures with wider canopy stripes. It is noteworthy that while the differences between the homogeneous and the striped structures are large, there are relatively small differences in canopy resistance at a given leaf area among the striped structures of different stripe spacing, at least within

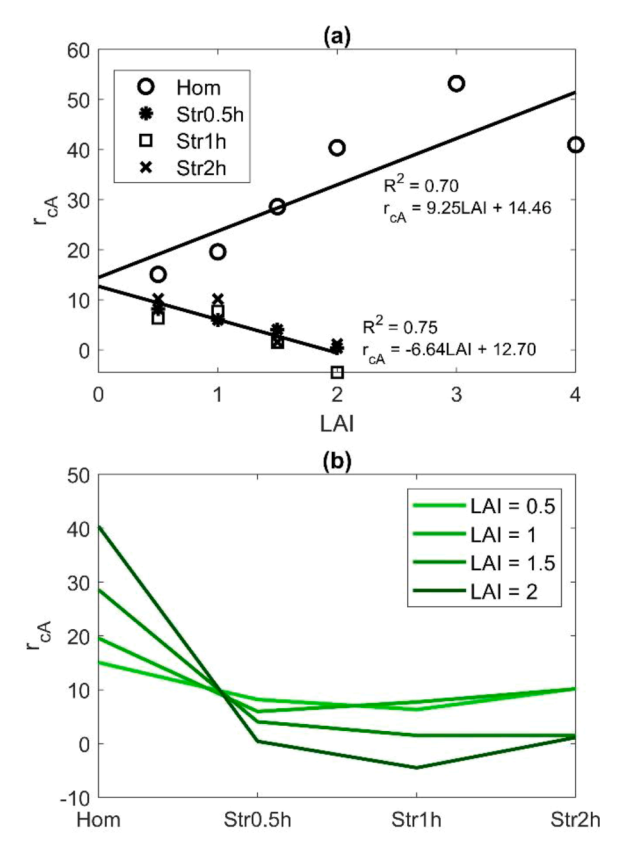


Fig. 10. (a) Canopy resistance per leaf area, r_{cA} , vs. LAI (a) and vs. Patch Type (b). Hom is Homogenous canopy, Str0.5h is narrow stripes canopies, Str1h is intermediate stripes canopy, and Str2h is wide stripes canopies.

the range that we tested, with stripe widths of 0.5h-2h.

5. Conclusion

We can design forested patches, especially in urban and industrial settings, to improve air quality by increasing the surface deposition flux of pollutants. However, in order to optimize the air quality regulation by greenbelts, we must understand the effects of the canopy structure and leaf density on the pollutant deposition rates. This LES-based virtual study was conducted in order to identify two characteristics of canopy structure, leaf area density and row spacing, on dry deposition of a passive scalar. Our results showed that more deposition occurred on denser canopies, however, adding leaves to homogenous canopies made them relatively less effective while adding leaves to striped canopy structures made them relatively more effective. We found that the driver of this effect of canopy structure lies in eddy-driven spatial covariance between wind speed, scalar concentration, and canopy structure. In striped canopies the sweep events became co-located with the gaps between the stripes, leading to more effective "recharge" of the canopy air. Air with higher scalar concentration from aloft was pushed into the canopy gaps and hit the backward pacing edges of the leaf rows at relatively high speed and high concentration, and thus, providing more deposition per leaf area. In homogenous canopies, the sweeps were less pronounced and the canopy air remained relatively clean, and within canopy wind speed remained low, providing less opportunities for deposition on leaf surfaces.

We used classic surface flux theory to relate our detailed, high-resolution simulation results to bulk, large-scale parameterization of surface conductivity to scalar flux. Increasing leaf area and changing the stripe spacing of the canopy structure affected the surface resistance beyond its first order effect on aerodynamic resistance. The parameter of canopy resistance per leaf area, r_{CA} , can be calculated from the simulation results and could be used as an additive term to standard B^{-1} parameterizations of surface resistance to account for canopy structure and leaf density effects. We showed that r_{CA} vary linearly with leaf area, and the slope (and direction) of that linear relationship depends on canopy structure. With a positive relationship in homogenous canopies and negative relationship in striped ones. The spacing of the stripes did not affect the slope of the relationship between r_{CA} and leaf area.

With additional simulations to create a more complete picture of the possible scenarios combining canopy structure, surface fluxes and meteorological conditions (see Supplementary Material), results could be used to improve the modeling of dry deposition on tree surfaces, by providing a leaf-area based correction to the surface conductance term. Improved understanding of dry deposition on tree surfaces could be used to optimize the synergy already present between forest ecosystem and air pollutants emitted by industrial complexes (Charles et al., 2020; Gopalakrishnan et al., 2019). Greenbelts downwind industrial sites could be planted in rows, noting that the trees with higher leaf area would be better since they would have more deposition. Such alternatives will facilitate efficient air quality regulation by forests and boost the techno-ecological synergy present between the forest ecosystem and industrial sites' emissions. It should be noted that our study does not apply only to industrial emissions but to any air pollutant that being is transported downwind a forest patch.

Declaration of Competing Interest

None.

Acknowledgments

The work was funded in part by the U.S. National Science Foundation projects 1508994, 2036982 and U.S. Department of Agriculture project NIFA-AFRI-20186701927803. TY was funded in part by a U.S. Fulbright Student Fellowship, CV and GB were funded in part by MICMOR

Graduate Student and Visiting Professor Fellowships from IFU-KIT Institute in Garmisch-Partenkirchen, Germany. Simulations were run at the Ohio Supercomputer Center with computational time allocation under project PAS0409. We thank PALM group at Leibniz University Hannover for the open access of PALM LES code that was used for performing the simulations.

Supplementary materials

Supplementary material associated with this article can be found, in the online version, at doi:10.1016/j.agrformet.2021.108440.

References

- Aylor, D.E., 2005. Quantifying maize pollen movement in a maize canopy. Agric. For. Meteorol. 131, 247–256. https://doi.org/10.1016/j.agrformet.2005.06.009.
- Banerjee, T., De Roo, F., Mauder, M., 2017. Explaining the convector effect in canopy turbulence by means of large-eddy simulation. Hydrol. Earth Syst. Sci. 21, 2987–3000. https://doi.org/10.5194/hess-21-2987-2017.
- Baró, F., Chaparro, L., Gómez-Baggethun, E., Langemeyer, J., Nowak, D.J., Terradas, J., 2014. Contribution of Ecosystem Services to Air Quality and Climate Change Mitigation Policies: The Case of Urban Forests in Barcelona. Spain. Ambio 43, 466–479. https://doi.org/10.1007/s13280-014-0507-x.
- Beckett, K.P., Freer-Smith, P.H., Taylor, G., 2001. Particulate pollution capture by urban trees: Effect of species and windspeed. Glob. Chang. Biol. 6, 995–1003. https://doi. org/10.1046/j.1365-2486.2000.00376.x.
- Bohrer, G., Katul, G.G., Nathan, R., Walko, R.L., Avissar, R., 2008. Effects of canopy heterogeneity, seed abscission and inertia on wind-driven dispersal kernels of tree seeds. J. Ecol. 96, 569–580. https://doi.org/10.1111/j.1365-2745.2008.01368.x.
- Bohrer, G., Katul, G.G., Walko, R.L., Avissar, R., 2009. Exploring the effects of microscale structural heterogeneity of forest canopies using large-eddy simulations. Boundary-Layer Meteorol 132, 351–382. https://doi.org/10.1007/s10546-009-9404-4.
- Bottalico, F., Chirici, G., Giannetti, F., De Marco, A., Nocentini, S., Paoletti, E., Salbitano, F., Sanesi, G., Serenelli, C., Travaglini, D., 2016. Air Pollution Removal by Green Infrastructures and Urban Forests in the City of Florence. Agric. Sci. Procedia 8, 243–251. https://doi.org/10.1016/j.aaspro.2016.02.099.
- Bou-Zeid, E., Meneveau, C., Parlange, M.B., 2004. Large-eddy simulation of neutral atmospheric boundary layer flow over heterogeneous surfaces: Blending height and effective surface roughness. Water Resour. Res. 40, 1–18. https://doi.org/10.1029/ 2003WR002475.
- Boughton, B.A., Delaurentis, J.M., Dunn, W.E., 1987. A stochastic model of particle dispersion in the atmosphere. Boundary-Layer Meteorol 40, 147–163. https://doi. org/10.1007/BF00140073.
- Brown, K.W., Covey, W., 1966. The energy-budget evaluation of the micrometeorological transfer processes within a cornfield. Agric. Meteorol. 3, 73–96. https://doi.org/
- Cassiani, M., Katul, G.G., Albertson, J.D., 2008. The effects of canopy leaf area index on airflow across forest edges: Large-eddy simulation and analytical results. Boundary-Layer Meteorol 126, 433–460. https://doi.org/10.1007/s10546-007-9242-1.
- Chamberlain, A.C., 1966. Transport of gases to and from grass and grass-like surfaces. Proc. R. Soc. A 290, 236–265. https://doi.org/10.1098/rspa.1966.0047.
- Charles, M., Ziv, G., Bohrer, G., Bakshi, B.R., 2020. Connecting air quality regulating ecosystem services with beneficiaries through quantitative serviceshed analysis. Ecosyst. Serv. 41, 101057 https://doi.org/10.1016/j.ecoser.2019.101057.
- Cherin, N., Roustan, Y., Musson-Genon, L., Seigneur, C., 2015. Modelling atmospheric dry deposition in urban areas using an urban canopy approach. Geosci. Model Dev. 8, 893–910. https://doi.org/10.5194/gmd-8-893-2015.
- Damschen, E.I., Baker, D.V., Bohrer, G., Nathan, R., Orrock, J.L., Turner, J.R., Brudvig, L. A., Haddad, N.M., Levey, D.J., Tewksbury, J.J., 2014. How fragmentation and corridors affect wind dynamics and seed dispersal in open habitats. Proc. Natl. Acad. Sci. U. S. A. 111, 3484–3489. https://doi.org/10.1073/pnas.1308968111.
- De Jong, J.J.M., Klaassen, W., 1997. Simulated dry deposition of nitric acid near forest edges. Atmos. Environ. 31, 3681–3691. https://doi.org/10.1016/S1352-2310(97)
- De Ridder, K., Neirynck, J., Mensink, C., 2004. Parameterising forest edge deposition using effective roughness length. Agric. For. Meteorol. 123, 1–11. https://doi.org/ 10.1016/j.agrformet.2003.11.007.
- De Schrijver, A., Devlaeminck, R., Mertens, J., Wuyts, K., Hermy, M., Verheyen, K., 2007. On the importance of incorporating forest edge deposition for evaluating exceedance of critical pollutant loads. Appl. Veg. Sci. 10, 293–298. https://doi.org/10.1111/j.1654-109X.2007.tb00529.x.
- Deardorff, J.W., 1980. Stratocumulus-capped mixed layers derived from a threedimensional model. Boundary-Layer Meteorol 18, 495–527. https://doi.org/ 10.1007/BF00119502.
- Dupont, S., Brunet, Y., 2009. Coherent structures in canopy edge flow: A large-eddy simulation study. J. Fluid Mech. 630, 93–128. https://doi.org/10.1017/ S0022112009006739.
- Dupont, S., Brunet, Y., 2008. Impact of forest edge shape on tree stability: A large-eddy simulation study. Forestry 81, 299–315. https://doi.org/10.1093/forestry/cpn006.
- Dupont, S., Patton, E.G., 2012. Momentum and scalar transport within a vegetation canopy following atmospheric stability and seasonal canopy changes: The CHATS

- experiment. Atmos. Chem. Phys. 12, 5913-5935. https://doi.org/10.5194/acp-12-5913-2012
- Erisman, J.W., Draaijers, G., 2003. Deposition to forests in Europe: Most important factors influencing dry deposition and models used for generalisation. Environ. Pollut. 124, 379–388. https://doi.org/10.1016/S0269-7491(03)00049-6.
- Escobedo, F., Wagner, J.E., Nowak, D.J., Maza, Luz De la, Carmen Rodriguez, M., Crane, D.E., 2008. Analyzing the cost effectiveness of Santiago, Chile's policy of using urban forests to improve air quality. J. Environ. Manage. 86, 148–157. https:// doi.org/10.1016/j.jenvman.2006.11.029.
- Finnigan, J.J., Shaw, R.H., Patton, E.G., 2009. Turbulence structure above a vegetation canopy. J. Fluid Mech. 637, 387–424. https://doi.org/10.1017/ S0022112009990589
- Freer-Smith, P.H., El-Khatib, A.A., Taylor, G., 2004. Capture of particulate pollution by trees: A comparison of species typical of semi-arid areas (Ficus Nitida and Eucalyptus Globulus) with European and North American species. Water. Air. Soil Pollut. 155, 173–187. https://doi.org/10.1023/B:WATE.0000026521.99552.fd.
- Gao, W., Shaw, R.H., Paw U, K.T., 1989. Observation of organized structure in turbulent flow within and above a forest canopy. Boundary-Layer Meteorol 47, 349–377. https://doi.org/10.1007/BF00122339.
- Garratt, J.R., Hicks, B.B., 1973. Momentum, heat and water vapour transfer to and from natural and artificial surfaces. Q. J. R. Meteorol. Soc. 99, 680–687. https://doi.org/ 10.1002/qj.49709942209.
- Gopalakrishnan, V., Bakshi, B.R., 2017. Including Nature in Engineering Decisions for Sustainability. Encycl. Sustain. Technol. 107–116. https://doi.org/10.1016/B978-0-12-409548-9 10039-9
- Gopalakrishnan, V., Bakshi, B.R., Ziv, G., 2016. Assessing the capacity of local ecosystems to meet industrial demand for ecosystem services. AIChE J. 62, 3319–3333. https://doi.org/10.1002/aic.15340.
- Gopalakrishnan, V., Ziv, G., Bakshi, B.R., 2019. Role of Vegetation in Mitigating Air Emissions Across Industrial Sites in the US. ACS Sustain. Chem. Eng. 7, 3783–3791. https://doi.org/10.1021/acssuschemeng.8b04360.
- Gromke, C., Ruck, B., 2012. Pollutant Concentrations in Street Canyons of Different Aspect Ratio with Avenues of Trees for Various Wind Directions. Boundary-Layer Meteorol 144, 41–64. https://doi.org/10.1007/s10546-012-9703-z.
- Gronholm, T., Launiainen, S., Ahlm, L., Martensson, E.M., Kulmala, M., Vesala, T., Nilsson, E.D., 2009. Aerosol particle dry deposition to canopy and forest floor measured by two-layer eddy covariance system. J. Geophys. Res. Atmos. 114, 1–12. https://doi.org/10.1029/2008JD010663.
- Grote, R., Samson, R., Alonso, R., Amorim, J.H., Cariñanos, P., Churkina, G., Fares, S., Le Thiec, D., Niinemets, Ü., Mikkelsen, T.N., Paoletti, E., Tiwary, A., Calfapietra, C., 2016. Functional traits of urban trees: air pollution mitigation potential. Front. Ecol. Environ. 14, 543–550. https://doi.org/10.1002/fee.1426.
- Hicks, B.B., 2008. On estimating dry deposition rates in complex terrain. J. Appl. Meteorol. Climatol. 47, 1651–1658. https://doi.org/10.1175/2006JAMC1412.1
- Hicks, B.B., Baldocchi, D.D., Meyers, T.P., R.P. Hosker, J., Matt, D.R., 1987.
 A Preliminary Multiple Resistance Routine for Deriving Dry Deposition Velocities
 From Measured Quantities. Water. Air. Soil Pollut. 36, 311–330. https://doi.org/10.1007/BF00229675
- Hicks, B.B., Saylor, R.D., Baker, B.D., 2016. Dry deposition of particles to canopies-A look back and the road forward. J. Geophys. Res. 121, 14691–14707. https://doi.org/ 10.1002/2015.ID024742.
- Hirabayashi, S., Kroll, C.N., Nowak, D.J., 2015. i-Tree Eco Dry Deposition Model Descriptions.
- Hirabayashi, S., Kroll, C.N., Nowak, D.J., 2012. Development of a distributed air pollutant dry deposition modeling framework. Environ. Pollut. 171, 9–17. https:// doi.org/10.1016/j.envpol.2012.07.002.
- Hirabayashi, S., Kroll, C.N., Nowak, D.J., 2011. Component-based development and sensitivity analyses of an air pollutant dry deposition model. Environ. Model. Softw. 26, 804–816. https://doi.org/10.1016/j.envsoft.2010.11.007.
- Huq, S., De Roo, F., Raasch, S., Mauder, M., 2018. Vertically nested LES for high-resolution simulation of the surface layer in PALM (version 5.0). Geosci. Model Dev. Discuss. 1–19. https://doi.org/10.5194/gmd-2018-287.
- Jones, N., Davies, C., 2017. Linking the Environmental, Social and Economic Aspects of Urban Forestry and Green Infrastructure. The Urban Forest. Springer, Cham, pp. 305–313. https://doi.org/10.1007/978-3-319-50280-9_23.
- Katul, G., Kuhn, G., Schieldge, J., Hsieh, C.I., 1997. The ejection-sweep character of scalar fluxes in the unstable surface layer. Boundary-Layer Meteorol 83, 1–26. https://doi.org/10.1023/A:1000293516830.
- Katul, G., Poggi, D., Cava, D., Finnigan, J., 2006. The relative importance of ejections and sweeps to momentum transfer in the atmospheric boundary layer. Boundary-Layer Meteorol 120, 367–375. https://doi.org/10.1007/s10546-006-9064-6.
- Katul, G.G., Grönholm, T., Launiainen, S., Vesala, T., 2011. The effects of the canopy medium on dry deposition velocities of aerosol particles in the canopy sub-layer above forested ecosystems. Atmos. Environ. 45, 1203–1212. https://doi.org/ 10.1016/j.atmosenv.2010.06.032.
- Kröniger, K., Banerjee, T., De Roo, F., Mauder, M., 2018. Flow adjustment inside homogeneous canopies after a leading edge – An analytical approach backed by LES. Agric. For. Meteorol. 255, 17–30. https://doi.org/10.1016/j. agrformet.2017.09.019.
- Kurppa, M., Hellsten, A., Auvinen, M., Raasch, S., Vesala, T., Järvi, L., 2018. Ventilation and air quality in city blocks using large-eddy simulation-urban planning perspective. Atmosphere (Basel) 9, 1–27. https://doi.org/10.3390/atmos9020065.
- Letzel, M.O., Helmke, C., Ng, E., An, X., Lai, A., Raasch, S., 2012. LES case study on pedestrian level ventilation in two neighbourhoods in Hong Kong. Meteorol. Zeitschrift 21, 575–589. https://doi.org/10.1127/0941-2948/2012/0356.

- Liu, X., Trogisch, S., He, J.S., Niklaus, P.A., Bruelheide, H., Tang, Z., Erfmeier, A., Scherer-Lorenzen, M., Pietsch, K.A., Yang, B., Kühn, P., Scholten, T., Huang, Y., Wang, C., Staab, M., Leppert, K.N., Wirth, C., Schmid, B., Ma, K., 2018. Tree species richness increases ecosystem carbon storage in subtropical forests. Proceedings. Biol. Sci. 285 https://doi.org/10.1098/rspb.2018.1240.
- Maronga, B., Banzhaf, S., Burmeister, C., Esch, T., Forkel, R., Fröhlich, D., Fuka, V., Gehrke, K.F., Geletić, J., Giersch, S., Gronemeier, T., Groß, G., Heldens, W., Hellsten, A., Hoffmann, F., Inagaki, A., Kadasch, E., Kanani-Sühring, F., Ketelsen, K., Ali Khan, B., Knigge, C., Knoop, H., Krč, P., Kurppa, M., Maamari, H., Matzarakis, A., Mauder, M., Pallasch, M., Pavlik, D., Pfafferott, J., Resler, J., Rissmann, S., Russo, E., Salim, M., Schrempf, M., Schwenkel, J., Seckmeyer, G., Schubert, S., Sühring, M., Von Tils, R., Vollmer, L., Ward, S., Witha, B., Wurps, H., Zeidler, J., Raasch, S., 2020. Overview of the PALM model system 6.0. Geoscientific Model Development. https://doi.org/10.5194/gmd-13-1335-2020.
- Maronga, B., Gryschka, M., Heinze, R., Hoffmann, F., Kanani-Sühring, F., Keck, M., Ketelsen, K., Letzel, M.O., Sühring, M., Raasch, S., 2015. The Parallelized Large-Eddy Simulation Model (PALM) version 4.0 for atmospheric and oceanic flows: Model formulation, recent developments, and future perspectives. Geosci. Model Dev. 8, 2515–2551. https://doi.org/10.5194/gmd-8-2515-2015.
- Meyers, T.P., Baldocchi, D.D., 1988. A comparison of models for deriving dry deposition fluxes of O3 and SO2 to a forest canopy. Tellus B Chem. Phys. Meteorol. 40, 270–284. https://doi.org/10.3402/tellusb.v40i4.15916.
- Meyers, T.P., Huebert, B.J., Hicks, B.B., 1989. HNO3 deposition to a deciduous forest. Boundary-Layer Meteorol 49, 395–410. https://doi.org/10.1007/BF00123651.
- Moeng, C.-H., Wyngaard, J.C., 1988. Spectral Analysis of large-Eddy Simulations of the Convective Boundary Layer. J. Atmos. Sci. 45, 3573–3587. https://doi.org/10.1175/1520-0469 (1988)045<3573:SAOLES>2.0.CO;2.
- Monteith, J.L., Unsworth, M.H., 1990. Principles of Environmental Physics: Plants, Animals, and the Atmosphere, 4th. Academic Press revised ed2013.
- Morakinyo, T.E., Lam, Y.F., 2016a. Study of traffic-related pollutant removal from street canyon with trees: dispersion and deposition perspective. Environ. Sci. Pollut. Res. 23, 21652–21668. https://doi.org/10.1007/s11356-016-7322-9.
- Morakinyo, T.E., Lam, Y.F., 2016b. Simulation study on the impact of tree-configuration, planting pattern and wind condition on street-canyon's micro-climate and thermal comfort. Build. Environ. 103, 262–275. https://doi.org/10.1016/j.buildenv.2016.04.025.
- NOAA/ESRL Radiosonde Database [WWW Document], 2021 URL https://ruc.noaa.gov/raobs/.
- Novick, Kim, Phillips, Rich, 2020. AmeriFlux US-MMS Morgan Monroe State Forest, Ver 18-5. Ameriflux AMP, (dataset). https://doi.org/10.17190/AMF/1246080.
- Nowak, D.J., 2002. The effects of urban trees on air quality. USDA Forest Service, Syracuse, NY.
- Nowak, D.J., Crane, D.E., 2000. The Urban Forest Effects (UFORE) model: quantifying urban forest structure and functions. eds.. In: Hansen, Mark, Burk, Tom (Eds.), Integrated tools for natural resources inventories in the 21st century. Gen. Tech. Rep. NC-212. St. Paul, MN: U.S. Dept. of Agriculture, Forest Service, North Central Forest Experiment Station.
- Nowak, D.J., Hirabayashi, S., Bodine, A., Greenfield, E., 2014. Tree and forest effects on air quality and human health in the United States. Environ. Pollut. 193 https://doi. org/10.1016/j.envpol.2014.05.028.
- Park, S.-B., Baik, J.-J., 2014. Large-Eddy Simulations of Convective Boundary Layers over Flat and Urbanlike Surfaces. J. Atmos. Sci. 71, 1880–1892. https://doi.org/ 10.1175/jas-d-13-0191.1.
- Patton, E.G., Horst, T.W., Sullivan, P.P., Lenschow, D.H., Oncley, S.P., Brown, W.O.J., Burns, S.P.P., Guenther, A.B., Held, A., Karl, T., Mayor, S.D., Rizzo, L.V., Spuler, S. M., Sun, J., Turnipseed, A.A., Awine, E.J., Edburg, S.L., Lamb, B.K., Avissar, R., Calhoun, R.J., Kleissl, J., Massman, W.J., Paw U, K.T., Weil, J.C., 2011. The canopy horizontal array turbulence study. Bull. Am. Meteorol. Soc. 92, 593–611. https:// doi.org/10.1175/2010BAMS2614.1.
- Petroff, A., Mailliat, A., Amielh, M., Anselmet, F., 2008. Aerosol dry deposition on vegetative canopies. Part I: Review of present knowledge. Atmos. Environ. 42, 3625–3653. https://doi.org/10.1016/j.atmosenv.2007.09.043.
- Pugh, T.A.M., MacKenzie, A.R., Whyatt, J.D., Hewitt, C.N., 2012. Effectiveness of green infrastructure for improvement of air quality in urban street canyons. Environ. Sci. Technol. 46, 7692–7699. https://doi.org/10.1021/es300826w.
- Raasch, S., Schröter, M., 2001. PALM A large-eddy simulation model performing on massively parallel computers. Meteorol. Zeitschrift 10, 363–372. https://doi.org/ 10.1127/0941-2948/2001/0010-0363.
- Raupach, M.R., 1989. Applying Lagrangian fluid mechanics to infer scalar source distributions from concentration profiles in plant canopies. Agric. For. Meteorol. 47, 85–108. https://doi.org/10.1016/0168-1923(89)90089-0.
- Raupach, M.R., Finnigan, J.J., Brunei, Y., 1996. Coherent eddies and turbulence in vegetation canopies: The mixing-layer analogy. Boundary-Layer Meteorol 78, 351–382. https://doi.org/10.1007/BF00120941.
- Raupach, M.R., Thom, A.S., 1981. Turbulence in and above Plant Canopies. Annu. Rev. Fluid Mech. 13, 97–129. https://doi.org/10.1146/annurev.fl.13.010181.000525.
- Resler, J., Krč, P., Belda, M., Juruš, P., Benešová, N., Lopata, J., Vlček, O., Damašková, D., Eben, K., Derbek, P., Maronga, B., Kanani-Sühring, F., 2017. PALM-USM v1.0: A new urban surface model integrated into the PALM large-eddy simulation model. Geosci. Model Dev. 10, 3635–3659. https://doi.org/10.5194/ omd-10-3635-2017
- Ross, A.N., 2008. Large-eddy simulations of flow over forested ridges. Boundary-Layer Meteorol 128, 59–76. https://doi.org/10.1007/s10546-008-9278-x.
- Ruijgrok, W., Tieben, H., Eisinga, P., 1997. The dry deposition of particles to a forest canopy: A comparison of model and experimental results. Atmos. Environ. 31, 399–415. https://doi.org/10.1016/S1352-2310(96)00089-1.

- Saiki, E.M., Moeng, C.H., Sullivan, P.P., 2000. Large-eddy simulation of the stably stratified planetary boundary layer. Boundary-Layer Meteorol 95, 1–30. https://doi. org/10.1023/A:1002428223156.
- Salmond, J.A., Williams, D.E., Laing, G., Kingham, S., Dirks, K., Longley, I., Henshaw, G. S., 2013. The influence of vegetation on the horizontal and vertical distribution of pollutants in a street canyon. Sci. Total Environ. 443, 287–298. https://doi.org/10.1016/j.scitotenv.2012.10.101.
- Shaw, R.H.R., Schumann, U., 1992. Large-eddy simulation of turbulent flow above and within a forest. Boundary-Layer Meteorol 61, 47–64. https://doi.org/10.1007/ BF02033994.
- Sutherland, D., Philip, J., Ooi, A., Moinuddin, K.A.M., 2018. Large eddy simulation of flow over streamwise heterogeneous canopies: Quadrant analysis. Australas. Fluid Mech. Conf. 21st
- Tetzlaff, G., Dlugi, R., Friedrich, K., Gross, G., Hinneburg, D., Pahl, U., Zelger, M., Mölders, N., 2002. On modeling dry deposition of long-lived and chemically reactive species over heterogeneous terrain. J. Atmos. Chem. 42, 123–155. https://doi.org/ 10.1023/A:1015740203204.

- Wania, A., Bruse, M., Blond, N., Weber, C., 2012. Analysing the influence of different street vegetation on traffic-induced particle dispersion using microscale simulations. J. Environ. Manage. 94, 91–101. https://doi.org/10.1016/j.jenvman.2011.06.036.
- Watanabe, T., 2004. Large-eddy simulation of coherent turbulence structures associated with scalar ramps over plant canopies. Boundary-Layer Meteorol 112, 307–341. https://doi.org/10.1023/B:BOUN.0000027912.84492.54.
- Wedding, J.B., Carlson, R.W., Stukel, J.J., Bazzaz, F.A., 1977. Aerosol deposition on plant leaves. Water. Air. Soil Pollut. 7, 545–550. https://doi.org/10.1007/BF00285551.
- Wesely, M.L., Hicks, B.B., 1977. Some factors that affect the deposition rates of sulfur dioxide and similar gases on vegetation. J. Air Pollut. Control Assoc. 27, 1110–1116. https://doi.org/10.1080/00022470.1977.10470534.
- Wiman, B.L.B., Ågren, G.I., 1985. Aerosol depletion and deposition in forests-A model analysis. Atmos. Environ. 19, 335–347. https://doi.org/10.1016/0004-6981(85) 90101-5.
- Wuyts, K., Verheyen, K., De Schrijver, A., Cornelis, W.M., Gabriels, D., 2008. The impact of forest edge structure on longitudinal patterns of deposition, wind speed, and turbulence. Atmos. Environ. 42, 8651–8660. https://doi.org/10.1016/j.atmosenv.2008.08.010.